# Performance Comparison of Massive MIMO Channel Models

Shangbin Wu[1], Cheng-Xiang Wang[2], Yang Yang[3], Wenjin Wang[4], and Xiqi Gao[4]
[1]Samsung R&D Institute UK, Staines-upon-Thames, TW18 4QE, UK.
[2]Institute of Sensors, Signals and Systems, School of Engineering & Physical Sciences, Heriot-Watt University, Edinburgh, EH14 4AS, UK.
[3]Key Lab of Wireless Sensor Network and Communication, Shanghai Research Center for Wireless Communications, SIMIT, Chinese Academy of Sciences, Shanghai 200050, China.
[4]National Mobile Communications Laboratory, Southeast University, Nanjing, Jiangsu 211189, China.
Email: shangbin.wu@samsung.com, cheng-xiang.wang@hw.ac.uk, yang.yang@wico.sh, wangwj@seu.edu.cn, xqgao@seu.edu.cn

***Abstract*—This paper compares the spatial cross-correlation functions (CCFs) and normalized channel capacities of four recently proposed massive multiple-input multiple-output (MIMO) channel models. Three of them are geometry-based stochastic models (GBSMs) and one is Kronecker-based stochastic model with birth death process on the array axis (KBSM-BD-AA). In addition, the impact of the elevation angles in the three dimensional (3-D) twin-cluster model and the 3-D unified GBSM on the resulting channel capacities, as well as the impact of polarization antennas in the 3-D unified GBSM on channel capacities, is investigated. Simulation results show that elevation angles can cause large impact on channel capacities and polarization antennas can halve the dimension of an antenna array at the cost of channel capacity loss.**

***Keywords* – Channel capacity, 2-D ellipse model, 3-D twin-cluster model, 3-D unified GBSM, KBSM-BD-AA.**

## I. Introduction

Specific characteristics of massive MIMO channels, such as cluster appearance and disappearance on the array axis and spherical wavefronts, can be found in measurements [1] [2]. Conventional MIMO channel models [3]–[5] cannot support these characteristics. Recently, a number of GBSMs were proposed for massive MIMO channels. The two dimensional (2-D) ellipse model [6] modeled the wideband massive MIMO channels by many confocal ellipses, which can be categorized as one of the regular shape channel models. On the other hand, the 3-D twin-cluster model [7] modeled each cluster as two representatives to characterized the first and last bounces. The complicated scattering environment was abstracted by a virtual link between the two representatives of a cluster. Both the 2-D ellipse model and 3-D twin-cluster model considered massive MIMO channel characteristics such as nearfield effects and non-stationary properties on the array axis. In addition, to satisfy emerging scenarios in the fifth generation (5G) mobile networks such as massive MIMO communications, high speed train (HST) communications, and machine-to-machine (M2M) communications, a unified GBSM framework combining the WINNER II channel model [4] and Saleh-Valenzuela channel model [8] for was proposed in [9]. Moreover, as the complexity of GBSMs for massive MIMO are relatively high, a low-complexity KBSM-BD-AA was proposed in [10].

Although statistical properties of the above-mentioned massive MIMO channel models [6], [7], [9], [10] have been studied, their channel capacities are missing in the literature. Therefore, in this report, channel capacities of these three models will be investigated.

The rest of this report is organized as follows. Section II describes the 2-D ellipse model, the 3-D twin-cluster model, the unified GBSM framework for massive MIMO channels, and the KBSM-BD-AA. Simulation results are studied in Section III. Conclusions are drawn in Section IV.

## II. Channel Models

### A. 2-D Ellipse Model

Let us assume that the transmitter and receiver are equipped with uniform linear arrays (ULAs) with $M_T$ and $M_R$ omnidirectional antennas and with antenna element separation of $\delta_T$ and $\delta_R$, respectively. They are located at the focal points of the confocal ellipses with a distance of $2f$. Let $\mathrm{Ant}_l^T$ represent the $l$-th antenna of the transmit array and $\mathrm{Ant}_k^R$ represent the $k$-th antenna of the receive array. The $n$-th cluster is on the $n$-th ellipse with major axis $2a_n$. The angle $\beta_T$ ($\beta_R$) denotes the tilt angle of the transmit (receive) antenna array. The angle $\alpha_v$ denotes the angle between the x-axis and the direction of movement of the receiver. The maximum Doppler frequency and carrier wavelength are denoted as $f_{\max}$ and $\lambda$, respectively.

Let $C_l^T$ ($C_k^R$) denote the cluster set in which clusters are observable to $\mathrm{Ant}_l^T$ ($\mathrm{Ant}_k^R$). The generation of $C_l^T$ and $C_k^R$ will be modeled as birth-death processes. Also, let $N_{\text{total}}$ denote the total number of clusters which are observable to at least one transmit antenna and one receive antenna. Here, $N_{\text{total}}$ can be expressed as [7]

$$N_{\text{total}} = \text{card}\left(\bigcup_{l=1}^{M_T}\bigcup_{k=1}^{M_R}\left(C_l^T(t)\bigcap C_k^R(t)\right)\right) \tag{1}$$

where the operator card$(\cdot)$ denotes the cardinality of a set. Then, a cluster, say $\mathrm{Cluster}_n$ $(n \leqslant N_{\text{total}})$, is observable to both $\mathrm{Ant}_l^T$ and $\mathrm{Ant}_k^R$ if and only if $\mathrm{Cluster}_n \in \left\{C_l^T \cap C_k^R\right\}$.

Based on the above mentioned analysis and the summary of key parameter definitions in Table I, the wideband ellipse

TABLE I
SUMMARY OF KEY PARAMETER DEFINITIONS FOR THE 2-D ELLIPSE MODEL.

| | |
|---|---|
| $\delta_T(\delta_R)$ | antenna spacing of the transmit (receive) antenna array |
| $M_T(M_R)$ | number of transmit (receive) antennas |
| $\beta_T(\beta_R)$ | title angles of the transmit (receive) antenna array |
| $f_{\max}$ | maximum Doppler frequency |
| $\lambda$ | carrier wavelength |
| $\mathrm{Ant}_l^T$, $\mathrm{Ant}_k^R$ | the $l$-th transmit antenna and the $k$-th receive antenna |
| $f_{kl}^{\mathrm{LOS}}$ | Doppler frequency of the LOS component between $k$-th receive antenna and the $l$-th transmit antenna |
| $f_{n,i}$ | Doppler frequency of the $n$-cluster via the $i$-th ray |
| $\varphi_{kl}^{\mathrm{LOS}}$ | phase of the LOS component between $k$-th receive antenna and the $l$-th transmit antenna |
| $\varphi_{kl,n,i}$ | phase of the $n$-th cluster between $k$-th receive antenna and the $l$-th transmit antenna via the $i$-th ray |

massive MIMO channel [6] can be presented as an $M_R \times M_T$ complex matrix $\mathbf{H}(t,\tau) = [h_{kl}(t,\tau)]_{M_R \times M_T}$, where $k = 1, 2, \cdots, M_R$ and $l = 1, 2, \cdots, M_T$. Next, assume the initial phase of the signal at the transmitter is $\varphi_0$, LOS Rician factor is $K$ and the LOS component is always connected to all antennas and the first cluster to arrive at the receiver if the LOS component exists. Additionally, assume that the mean power of the $n$-th cluster is $P_n$ and there are $S$ rays within one cluster and $\alpha_{n,i}^R$ is the AoA of the $i$-th ray of the $n$-th cluster to the receive array center, $\alpha_{n,i}^T$ is the AoD of the $i$-th ray of the $n$-th cluster ($i = 1, 2, \cdots, S$) to the transmit array center, the multipath complex gains $h_{kl}(t,\tau)$ of the theoretical model ($S \to \infty$) between $\mathrm{Ant}_l^T$ and $\mathrm{Ant}_k^R$ at delay $\tau$ can be presented as

$$h_{kl}(t,\tau) = \sum_{n=1}^{N_{\text{total}}} h_{kl,n}(t)\delta(\tau - \tau_n) \tag{2}$$

where the complex gain $h_{kl,n}(t)$ of $\mathrm{Cluster}_n$ can be computed as

-if $\mathrm{Cluster}_n \in \{C_l^T \cap C_k^R\}$,

$$h_{kl,n}(t) = \underbrace{\delta(n-1)\sqrt{\frac{K}{K+1}}e^{j\left(2\pi f_{kl}^{\mathrm{LOS}} t + \varphi_{kl}^{\mathrm{LOS}}\right)}}_{\mathrm{LOS}} + \underbrace{\sqrt{\frac{P_n}{K+1}}\lim_{S\to\infty}\frac{1}{\sqrt{S}}\sum_{i=1}^{S} e^{j(2\pi f_{n,i}t + \varphi_{kl,n,i})}}_{\mathrm{NLOS}} \tag{3}$$

-if $\mathrm{Cluster}_n \notin \{C_l^T \cap C_k^R\}$,

$$h_{kl,n}(t) = 0. \tag{4}$$

The detailed calculations of parameters in Table I of the 2-D ellipse model can be found in [6].

### B. 3-D Twin-cluster Model

Next, let us consider a wideband massive MIMO system with multiple twin clusters in a 3-D space to describe different taps of the channel. For a twin-cluster channel model with $N_{\text{total}}$ clusters, each cluster, say $\mathrm{Cluster}_n$ ($n = 1, \ldots, N_{\text{total}}$), is made of a representation $\mathrm{Cluster}_n^T$ at the transmitter side denoting the first bounce and a representation $\mathrm{Cluster}_n^R$ at the receiver side denoting the last bounce. The propagation environment between these two representations is abstracted as a virtual link.

Let us assume that the transmitter and receiver are equipped with ULAs with $M_T$ and $M_R$ antenna elements, respectively. The distances between antenna elements are $\delta_T$ at the transmitter and $\delta_R$ at the receiver. Let the transmitter be the origin of the 3D space, the distance vector between the transmitter and receiver is $\mathbf{D} = (D, 0, 0)$.

Next, let us denote the maximum Doppler frequency as $f_{\max}$, the LOS Rician factor as $K$, and the initial phase of the signal at the transmitter as $\varphi_0$. Additionally, let us assume that the power of the $n$-th cluster is $P_n$ and there are respectively $S_1$ and $S_2$ rays within the representation at the receiver side and the representation at the transmitter side. Based on geometrical parameters in Table II, as $S_1, S_2 \to \infty$, the theoretical model of the wideband twin-cluster massive MIMO channel [7] matrix can be represented as an $M_R \times M_T$ complex matrix $\mathbf{H}(t,\tau) = [h_{kl}(t,\tau)]_{M_R \times M_T}$ where $k = 1, 2, ..., M_R$ and $l = 1, 2, ..., M_T$. The multipath complex gains between the $l$-th transmit antenna and the $k$-th receive antenna at time $t$ and delay $\tau$, $h_{kl}(t,\tau)$, can be presented as

$$h_{kl}(t,\tau) = \sum_{n=1}^{N_{\text{total}}} h_{kl,n}(t)\delta(\tau - \tau_n(t)) \tag{5}$$

-if $\mathrm{Cluster}_n \in \{C_l^T(t) \cap C_k^R(t)\}$,

$$h_{kl,n}(t) = \underbrace{\delta(n-1)\sqrt{\frac{K}{K+1}}e^{j\left(2\pi f_{kl}^{\mathrm{LOS}} t + \varphi_{kl}^{\mathrm{LOS}}\right)}}_{\mathrm{LOS}} + \underbrace{\sqrt{\frac{P_n}{K+1}}\lim_{S_1,S_2\to\infty}\sum_{i_1=1}^{S_1}\sum_{i_2=1}^{S_2}\frac{e^{j\left(2\pi f_{kn,i_1}t + \varphi_{kl,n,i_1 i_2}\right)}}{\sqrt{S_1 S_2}}}_{\mathrm{NLOS}} \tag{6}$$

-if $\mathrm{Cluster}_n \notin \{C_l^T(t) \cap C_k^R(t)\}$,

$$h_{kl,n}(t) = 0. \tag{7}$$

The detailed calculations of parameters in Table II of the 3-D twin-cluster model can be found in [7].

### C. 3-D Unified GBSM Framework

Let us consider a MIMO system with $M_R$ receive and $M_T$ transmit antennas communicating at carrier frequency $f_c$.

TABLE II
DEFINITIONS OF KEY GEOMETRY PARAMETERS FOR THE 3-D TWIN-CLUSTER MODEL.

| | |
|---|---|
| $\upsilon_E^R$ | elevation angles of the receive antenna array |
| $\upsilon_E^T$ | elevation angles of the transmit antenna array |
| $\upsilon_A^R$ | azimuth angles of the receive antenna array |
| $\upsilon_A^T$ | azimuth angles of the transmit antenna array |
| $\xi_{n,i_1}^R$ | elevation angle of the $i_1$-th ray of the $n$-th cluster at the receiver side |
| $\theta_{n,i_1}^R$ | azimuth angle of the $i_1$-th ray of the $n$-th cluster at the receiver side |
| $\xi_{n,i_2}^T$ | elevation angle of the $i_2$-th ray of the $n$-th cluster at the transmitter side |
| $\theta_{n,i_2}^T$ | azimuth angle of the $i_2$-th ray of the $n$-th cluster at the transmitter side |

Let $\mathrm{Ant}_q^R$ denote the $q$th receive antenna and $\mathrm{Ant}_p^T$ denote the $p$th transmit antenna ($1 \le q \le M_R, 1 \le p \le M_T$). Uniform linear arrays with receive antenna spacing $\delta_R$ and transmit antenna spacing $\delta_T$ are assumed for description convenience. Antenna responses can be modified subject to actual antenna settings. The scattering environment between the transmitter and receiver is abstracted as effective clusters, which characterize the first and last bounces of the channel.

Given the key geometrical parameters listed in Table III, the position vectors of $\mathrm{Ant}_q^R$ and $\mathrm{Ant}_p^T$ can be expressed as

$$\mathbf{A}_q^R(t) = \frac{M_R - 2q + 1}{2}\delta_R \begin{bmatrix} \cos\upsilon_E^R(t)\cos\upsilon_A^R(t) \\ \cos\upsilon_E^R(t)\sin\upsilon_A^R(t) \\ \sin\upsilon_E^R(t) \end{bmatrix}^{\mathrm{T}} + \mathbf{D} \quad (8)$$

$$\mathbf{A}_p^T(t) = \frac{M_T - 2p + 1}{2}\delta_T \begin{bmatrix} \cos\upsilon_E^T(t)\cos\upsilon_A^T(t) \\ \cos\upsilon_E^T(t)\sin\upsilon_A^T(t) \\ \sin\upsilon_E^T(t) \end{bmatrix}^{\mathrm{T}} \quad (9)$$

respectively, where $\mathbf{D}$ is assumed to equal $[D, 0, 0]^{\mathrm{T}}$ and $D$ is the initial distance between the transmitter and receiver. The LOS distance vector $\mathbf{D}_{qp}^{\mathrm{LOS}}(t)$ between $\mathrm{Ant}_q^R$ and $\mathrm{Ant}_p^T$ is computed as

$$\mathbf{D}_{qp}^{\mathrm{LOS}}(t) = \mathbf{A}_q^R(t) - \mathbf{A}_p^T(t). \quad (10)$$

Distance vectors of $\mathrm{Cluster}_n$ at the transmitter and receiver are calculated as

$$\mathbf{D}_n^R(t) = D_n^R(t) \begin{bmatrix} \cos\phi_n^E(t)\cos\phi_n^A(t) \\ \cos\phi_n^E(t)\sin\phi_n^A(t) \\ \sin\phi_n^E(t) \end{bmatrix}^{\mathrm{T}} + \mathbf{D} \quad (11)$$

$$\mathbf{D}_n^T(t) = D_n^T(t) \begin{bmatrix} \cos\varphi_n^E(t)\cos\varphi_n^A(t) \\ \cos\varphi_n^E(t)\sin\varphi_n^A(t) \\ \sin\varphi_n^E(t) \end{bmatrix}^{\mathrm{T}} \quad (12)$$

where $D_n^R(t)$ and $D_n^T(t)$ are the Frobenius norms of $\mathbf{D}_n^R(t)$ and $\mathbf{D}^T n(t)$, respectively. Distance vectors of the $m_n$th ray of $\mathrm{Cluster}_n$ to the transmitter and receiver center are calculated as

$$\mathbf{D}_{n,m_n}^R(t) = D_n^R(t) \begin{bmatrix} \cos\phi_{n,m_n}^E(t)\cos\phi_{n,m_n}^A(t) \\ \cos\phi_{n,m_n}^E(t)\sin\phi_{n,m_n}^A(t) \\ \sin\phi_{n,m_n}^E(t) \end{bmatrix}^{\mathrm{T}} + \mathbf{D} \quad (13)$$

$$\mathbf{D}_{n,m_n}^T(t) = D_n^T(t) \begin{bmatrix} \cos\varphi_{n,m_n}^E(t)\cos\varphi_{n,m_n}^A(t) \\ \cos\varphi_{n,m_n}^E(t)\sin\varphi_{n,m_n}^A(t) \\ \sin\varphi_{n,m_n}^E(t) \end{bmatrix}^{\mathrm{T}}. \quad (14)$$

Distance vectors between the $m_n$th ray of $\mathrm{Cluster}_n$ and antenna elements are calculated as

$$\mathbf{D}_{qn,m_n}^R(t) = \mathbf{D}_{n,m_n}^R(t) - \mathbf{A}_q^R(t) \quad (15)$$

$$\mathbf{D}_{pn,m_n}^T(t) = \mathbf{D}_{n,m_n}^T(t) - \mathbf{A}_p^T(t). \quad (16)$$

The unified GBSM framework at time $t$ with delay $\tau$ can be characterized by an $M_R \times M_T$ matrix $\mathbf{H}(t,\tau) = [h_{qp}(t,\tau)]$. The entries of $\mathbf{H}(t,\tau)$ consist of two components, i.e., the LOS component and the NLOS component, and can be written as

$$h_{qp}(t,\tau) = \underbrace{\sqrt{\frac{K(t)}{K(t)+1}} h_{qp}^{\mathrm{LOS}}(t)\delta\left(\tau - \tau^{\mathrm{LOS}}(t)\right)}_{\mathrm{LOS}} + \underbrace{\sqrt{\frac{1}{K(t)+1}} \sum_{n=1}^{N(t)} \sum_{m_n=1}^{M_n(t)} h_{qp,n,m_n}(t)\delta\left(\tau - \tau_n(t) - \tau_{m_n}(t)\right)}_{\mathrm{NLOS}}. \quad (17)$$

In (17), $K(t)$ is the Rician factor, $N(t)$ is the time variant number of clusters, $M_n(t)$ is the number of rays within $\mathrm{Cluster}_n$, $\tau_n(t)$ is the delay of $\mathrm{Cluster}_n$ and $\tau_{m_n}(t)$ is the relative delay of the $m_n$th ray in $\mathrm{Cluster}_n$. To simplify the channel model, we assume that the Rician factor and relative delays are constants, i.e., $K(t) = K$ and $\tau_{m_n}(t) = \tau_{m_n}$. Also, the number of rays within a cluster is assumed to follow a Poisson distribution $\mathrm{Pois}\left(\tilde{\lambda}\right)$, i.e., $M_n(t) = M_n = \max\left\{\mathrm{Pois}\left(\tilde{\lambda}\right), 1\right\}$, where $\tilde{\lambda}$ is both the mean and variance of $M_n$ and $\max\{\cdot\}$ calculates the maximum value.

For the LOS component, if polarized antenna arrays are assumed at both the receiver and transmitter sides, the complex channel gain $h_{qp}^{\mathrm{LOS}}(t)$ is presented as (18) where $\Phi_{\mathrm{LOS}}^{\mathrm{VV}}$ and $\Phi_{\mathrm{LOS}}^{\mathrm{HH}}$ are uniformly distributed within $(0, 2\pi)$. The superscripts V and H denote vertical polarization and horizontal polarization, respectively. Antenna patterns $F^T(\cdot,\cdot)$ and $F^R(\cdot,\cdot)$ can be modified according to practical antenna pattern settings. The Doppler frequency $f_{qp}^{\mathrm{LOS}}(t)$ between $\mathrm{Ant}_q^R$ and $\mathrm{Ant}_p^T$ of the LOS component is expressed as

$$f_{qp}^{\mathrm{LOS}}(t) = \frac{1}{\lambda}\frac{\left\langle \mathbf{D}_{qp}^{\mathrm{LOS}}(t), \mathbf{v}^R - \mathbf{v}^T \right\rangle}{\left\| \mathbf{D}_{qp}^{\mathrm{LOS}}(t) \right\|} \quad (19)$$

where $\langle\cdot,\cdot\rangle$ is the inner product operator, $\|\cdot\|$ calculates the Frobenius norm, and $\lambda$ is the wavelength of the carrier. Given

TABLE III
DEFINITIONS OF KEY GEOMETRY PARAMETERS FOR THE 3-D UNIFIED GBSM FRAMEWORK.

| | |
|---|---|
| $\upsilon_A^R(t)$, $\upsilon_E^R(t)$ | azimuth and elevation angles of the receive array |
| $\upsilon_A^T(t)$, $\upsilon_E^T(t)$ | azimuth and elevation angles of the transmit array |
| $\phi_n^A(t)$, $\phi_n^E(t)$ | central azimuth and elevation angles between $\mathrm{Cluster}_n$ and the receive array |
| $\varphi_n^A(t)$, $\varphi_n^E(t)$ | central azimuth and elevation angles between $\mathrm{Cluster}_n$ and the transmit array |
| $\phi_{n,m_n}^A(t)$, $\phi_{n,m_n}^E(t)$ | central azimuth and elevation angles between the $m_n$th ray of $\mathrm{Cluster}_n$ and the receive array |
| $\varphi_{n,m_n}^A(t)$, $\varphi_{n,m_n}^E(t)$ | central azimuth and elevation angles between the $m_n$th ray of $\mathrm{Cluster}_n$ and the transmit array |
| $\mathbf{A}_q^R(t)$, $\mathbf{A}_p^T(t)$ | 3-D position vectors of $\mathrm{Ant}_q^R$ and $\mathrm{Ant}_p^T$ |
| $\mathbf{D}_n^R(t)$, $\mathbf{D}_n^T(t)$ | 3-D distance vectors between $\mathrm{Cluster}_n$ and the receiver (transmitter) array center |
| $\mathbf{D}_{n,m_n}^R(t)$,$\mathbf{D}_{n,m_n}^T(t)$ | 3-D distance vectors between $\mathrm{Cluster}_n$ and the receive (transmit) array center via the $m_n$th ray |
| $\mathbf{D}_{qn,m_n}^R(t)$,$\mathbf{D}_{pn,m_n}^T(t)$ | 3-D distance vectors between $\mathrm{Cluster}_n$ and $\mathrm{Ant}_q^R$ ($\mathrm{Ant}_p^T$) via the $m_n$th ray |
| $f_{qn,m_n}^R(t)$,$f_{pn,m_n}^T(t)$ | Doppler frequencies of $\mathrm{Ant}_q^R$ ($\mathrm{Ant}_p^T$) via $\mathrm{Cluster}_n$ and the $m_n$th ray |
| $\mathbf{D}_{qp}^{\mathrm{LOS}}(t)$ | 3-D distance vector of the LOS component between $\mathrm{Ant}_q^R$ and $\mathrm{Ant}_p^T$ |
| $f_{pq}^{\mathrm{LOS}}(t)$ | Doppler frequency of the LOS component between $\mathrm{Ant}_q^R$ and $\mathrm{Ant}_p^T$ |
| $\mathbf{v}^R$,$\mathbf{v}^T$ | 3-D velocity vectors of the receive and transmit arrays |
| $\mathbf{v}_n^R$, $\mathbf{v}_n^T$ | 3-D velocity vectors of the last bounce and first bounce of $\mathrm{Cluster}_n$ |
| $P_{n,m_n}(t)$ | mean power of the $m_n$th ray of $\mathrm{Cluster}_n$ |
| $\mathbf{D}$ | 3-D distance vector between the receive and transmit array centers |

$$h_{qp}^{\mathrm{LOS}}(t)=\begin{bmatrix}F_{p,\mathrm{V}}^T(\mathbf{D}_{qp}^{\mathrm{LOS}}(t),\mathbf{A}_p^T(t))\\ F_{p,\mathrm{H}}^T(\mathbf{D}_{qp}^{\mathrm{LOS}}(t),\mathbf{A}_p^T(t))\end{bmatrix}^{\mathrm{T}}\begin{bmatrix}e^{j\Phi_{\mathrm{LOS}}^{\mathrm{VV}}} & 0\\ 0 & e^{j\Phi_{\mathrm{LOS}}^{\mathrm{HH}}}\end{bmatrix}\begin{bmatrix}F_{q,\mathrm{V}}^R(\mathbf{D}_{qp}^{\mathrm{LOS}}(t),\mathbf{A}_q^R(t))\\ F_{q,\mathrm{H}}^R(\mathbf{D}_{qp}^{\mathrm{LOS}}(t),\mathbf{A}_q^R(t))\end{bmatrix}e^{j2\pi f_{qp}^{\mathrm{LOS}}(t)t}e^{j\Phi_{qp}^{\mathrm{LOS}}(t)} \tag{18}$$

the initial phase $\Phi_0$ and the speed of light $c$, the phase $\Phi_{qp}^{\mathrm{LOS}}(t)$ and delay $\tau^{\mathrm{LOS}}(t)$ of the LOS component are computed as

$$\Phi_{qp}^{\mathrm{LOS}}(t)=\Phi_0+\frac{2\pi}{\lambda}\left\|\mathbf{D}_{qp}^{\mathrm{LOS}}(t)\right\| \tag{20}$$

$$\tau^{\mathrm{LOS}}(t)=\left\|\mathbf{D}(t)\right\|/c. \tag{21}$$

For NLOS components, if $\mathrm{Cluster}_n$ is observable to $\mathrm{Ant}_q^R$ and $\mathrm{Ant}_p^T$, i.e., $\mathrm{Cluster}_n\in S_{qp}(t)$, the complex channel gain is expressed as (22) where $P_{n,m_n}$ is the normalized mean power of the $m_n$th ray in $\mathrm{Cluster}_n$. The normalized mean power of $\mathrm{Cluster}_n$ can be calculated as $P_n=\sum_{m_n}P_{n,m_n}$. Random phases $\Phi_{n,m_n}^{\mathrm{VV}},\Phi_{n,m_n}^{\mathrm{VH}},\Phi_{n,m_n}^{\mathrm{HV}},\Phi_{n,m_n}^{\mathrm{HH}}$ are uniformly distributed over $(0,2\pi)$.

Conversely, if $\mathrm{Cluster}_n$ is not observable, i.e., $\mathrm{Cluster}_n\notin S_{qp}(t)$, the complex channel gain

$$h_{qp,n,m_n}(t)=0. \tag{23}$$

Accordingly, the Doppler frequencies at the receiver and transmitter are calculated as

$$f_{qn,m_n}^R(t)=\frac{1}{\lambda}\frac{\left\langle\mathbf{D}_{qn,m_n}^R(t),\mathbf{v}^R-\mathbf{v}_n^R\right\rangle}{\left\|\mathbf{D}_{qn,m_n}^R(t)\right\|} \tag{24}$$

$$f_{pn,m_n}^T(t)=\frac{1}{\lambda}\frac{\left\langle\mathbf{D}_{pn,m_n}^T(t),\mathbf{v}^T-\mathbf{v}_n^T\right\rangle}{\left\|\mathbf{D}_{pn,m_n}^T(t)\right\|}. \tag{25}$$

Moreover, the phase $\Phi_{qp,n,m_n}(t)$ and delay $\tau_n(t)$ of the NLOS component are computed as

$$\Phi_{qp,n,m_n}(t)=\Phi_0+\frac{2\pi}{\lambda}\left[\left\|\mathbf{D}_{qn,m_n}^R(t)\right\|+\left\|\mathbf{D}_{pn,m_n}^T(t)\right\|\right] \tag{26}$$

$$\tau_n(t)=\left[\left\|\mathbf{D}_n^R(t)\right\|+\left\|\mathbf{D}_n^T(t)\right\|\right]/c+\tilde{\tau}_n(t) \tag{27}$$

where $\tilde{\tau}_n(t)$ is an exponentially distributed random variable representing the virtual delay between the first and last bounces of $\mathrm{Cluster}_n$ in the scattering environment.

### D. KBSM–BD–AA

The conventional KBSM assumes that spatial correlation matrices of the receive arrays and transmit arrays are unrelated. Hence, the channel matrix can be expressed as

$$\mathbf{H}=\mathbf{R}_R^{\frac{1}{2}}\mathbf{H}_{\mathrm{w}}\mathbf{R}_T^{\frac{\mathrm{T}}{2}} \tag{28}$$

where $\mathbf{H}_{\mathrm{w}}$ is an $M_R\times M_T$ matrix with zero-mean unit-variance complex i.i.d Gaussian entries, $\mathbf{R}_R$ and $\mathbf{R}_T$ are overall spatial correlation matrices at the receiver and transmitter, respectively. Additionally, if ULAs are deployed at the receiver and transmitter sides, $\mathbf{R}_R$ and $\mathbf{R}_T$ are Toeplitz matrices [11]. To avoid repeated analysis, we only analyze the receiver side in this paper as the analysis of the transmitter side follows the same procedure. Furthermore, let us denote the complex gain between the $k$th ($k=1,2,\cdots$) scatterer and the $m$th ($m=1,2,\cdots,M_R$) antenna as $s_{mk}^R$, and the complex gain between the $k$th scatterer and the $n$th ($n=1,2,\cdots,M_R$) antenna as $s_{nk}^R$. Let $T_{R,mn}$ be the spatial correlation coefficient between the $m$th and the $n$th antennas and the entry of matrix $\mathbf{T}_R$ in the $m$th row and $n$th column. Then, $T_{R,mn}$ can be computed as

$$T_{R,mn}=\frac{\sum_k s_{mk}^R\left(s_{nk}^R\right)^*}{\sqrt{\sum_k|s_{mk}^R|^2}\sqrt{\sum_k|s_{nk}^R|^2}}. \tag{29}$$

$$h_{qp,n,m_n}(t) = \begin{bmatrix} F_{p,\mathrm{V}}^{T}(\mathbf{D}_{n,m_n}^{T}(t), \mathbf{A}_{p}^{T}(t)) \\ F_{p,\mathrm{H}}^{T}(\mathbf{D}_{n,m_n}^{T}(t), \mathbf{A}_{p}^{T}(t)) \end{bmatrix}^{\mathrm{T}} \begin{bmatrix} e^{j\Phi_{n,m_n}^{\mathrm{VV}}} & \sqrt{\kappa} e^{j\Phi_{n,m_n}^{\mathrm{VH}}} \\ \sqrt{\kappa} e^{j\Phi_{n,m_n}^{\mathrm{HV}}} & e^{j\Phi_{n,m_n}^{\mathrm{HH}}} \end{bmatrix} \begin{bmatrix} F_{q,\mathrm{V}}^{R}(\mathbf{D}_{n,m_n}^{R}(t), \mathbf{A}_{q}^{R}(t)) \\ F_{q,\mathrm{H}}^{R}(\mathbf{D}_{n,m_n}^{R}(t), \mathbf{A}_{q}^{R}(t)) \end{bmatrix} \times \sqrt{P_{n,m_n}(t)} e^{j2\pi f_{qn,m_n}^{R}(t)t} e^{j2\pi f_{pn,m_n}^{T}(t)t} e^{j\Phi_{qp,n,m_n}(t)} \tag{22}$$

In the conventional KBSM, the above discussion implies that all the antennas share the same set of scatterers. In this case, $\mathbf{R}_R$ is equivalent to $\mathbf{T}_R$, i.e., $\mathbf{T}_R = \mathbf{R}_R$. However, the equivalence between $\mathbf{T}_R$ and $\mathbf{R}_R$ may not hold if antennas do not share the same set of scatterers. This will be studied in later paragraphs.

It was reported in [1] and [2] that each antenna on a large antenna array may not observe the same set of scatterers. Scatterers may appear or disappear on the array axis. As a result, for massive MIMO, different antennas may observe different scatters. The KBSM–BD–AA in [10] is developed to characterize this effect for massive MIMO channels. According to the BD process, the survival probability $E_{R,mn}$ of scatterers when they evolve from the $m$th antenna to the $n$th antenna can be modeled as an exponential function [10]

$$E_{R,mn} = e^{-\beta|m-n|} \tag{30}$$

where $\beta \geqslant 0$ is a parameter describing how fast a scatterer disappears on the array axis. The value of $E_{R,mn}$ is decreasing if $m$ and $n$ differ more. This implies that less scatterers are shared if two antennas are more separated. Let $T'_{R,mn}$ be the antenna correlation between the $m$th and $n$th antennas considering the evolution of scatterer sets on the array axis. Then, $T'_{R,mn}$ can be modeled as

$$T'_{R,mn} = E_{R,mn} \frac{\sum_k s_{mk}^{R} \left(s_{nk}^{R}\right)^{*}}{\sqrt{\sum_k |s_{mk}^{R}|^2} \sqrt{\sum_k |s_{nk}^{R}|^2}} = E_{R,mn} T_{R,mn}. \tag{31}$$

It can be observed that the antenna correlation of KBSM–BD–AA for massive MIMO is equal to the antenna correlation of KBSM for conventional MIMO multiplied by a factor of $E_{R,mn}$. This is because only $E_{R,mn}$ of the scatterers for the $m$th antenna are able to survive to be observed by the $n$th antenna. At the same time, although there may be new scatterers generated according to the BD process, these newly generated scatterers are uncorrelated to the survived scatterers. Therefore, the newly generated scatterers do not contribute to the antenna correlation. Let $\mathbf{E}_R = [E_{R,mn}]_{M_R \times M_R}$ $(m, n = 1, 2, \cdots, M_R)$ and $\mathbf{E}_T = [E_{T,pq}]_{M_T \times M_T}$ $(p, q = 1, 2, \cdots, M_T)$ denote the survival probability matrices at the receiver side and transmitter side. The overall antenna correlation matrices $\mathbf{R}_R$ and $\mathbf{R}_T$ can be represented as $\mathbf{R}_R = \mathbf{T}_R \circ \mathbf{E}_R$ and $\mathbf{R}_T = \mathbf{T}_T \circ \mathbf{E}_T$ where $\circ$ denotes the Hadamard product.

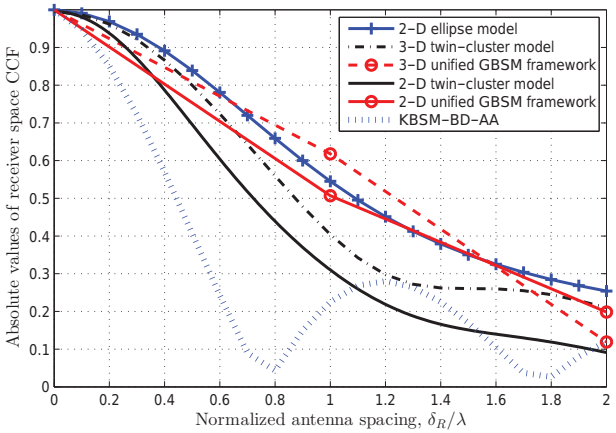


Fig. 1. Receiver correlation functions of three channel models ($M_R = 8$, $M_T = 32$, $f_c = 2$GHz, $\|\mathbf{D}\| = 100$m, $\upsilon_A^R = \frac{\pi}{4}$, $\upsilon_A^T = \frac{\pi}{3}$, $\upsilon_E^R = \frac{\pi}{4}$ (3-D models only), $\upsilon_E^T = \frac{\pi}{4}$ (3-D models only)).

## III. Results and Analysis

Absolute values of receiver space CCFs of the 2-D ellipse, 3-D twin-cluster massive MIMO channel model, 3-D unified GBSM, and KBSM-BD-AA (isotropic scattering environment) are shown in Fig. 1. It can be observed that the spatial correlation of the 2-D twin-cluster model is slightly smaller than that of the 3-D twin-cluster model. The same observation applies to the 3-D unified GBSM. The CCF of the KBSM-BD-AA in isotropic scattering environments is the product of the zero-th order Bessel function of the first kind and an exponentially decaying function.

Fig. 2 depicts the channel capacities of the i.i.d. massive MIMO channel model, KBSM-BD-AA (isotropic scattering environment), 2-D ellipse, 3-D twin-cluster, reduced 2-D twin-cluster massive MIMO channel model, 3-D unified GBSM, and reduced 2-D unified GBSM. The channel capacities of those three GBSMs slightly vary with elevation angles considered. The i.i.d. channel model serves as the upper bound of channel capacities. Also, channel capacities of all these models are comparable when the SNR is less than 12 dB.

The channel capacities of the 3-D twin-cluster channel model and the 3-D unified GBSM with different receiver elevation angles are compared in Fig. 3. The trend of the channel capacity of the 3-D twin-cluster channel model is similar to that of the 3-D unified GBSM. With various receiver angles, the channel capacities fluctuate approximately 7%. Therefore, it is necessary to consider elevation angles in 3-D models for accurate evaluation of system performance.

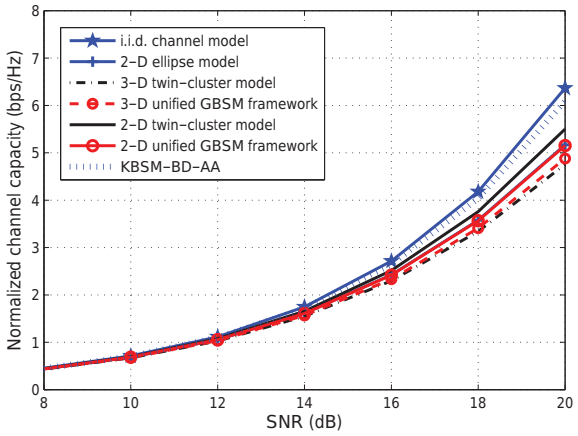


Fig. 2. Comparison of channel capacities of the i.i.d. massive MIMO channel model, the 2-D ellipse massive MIMO channel model, the 3-D twin-cluster massive MIMO channel model, and the 3-D unified GBSM framework for massive MIMO ($M_R = 8$, $M_T = 32$, $f_c = 2$GHz, $\|\mathbf{D}\| = 100$m, $\upsilon_A^R = \frac{\pi}{4}$, $\upsilon_A^T = \frac{\pi}{3}$, $\upsilon_E^R = \frac{\pi}{4}$ (3-D models only), $\upsilon_E^T = \frac{\pi}{4}$ (3-D models only)).

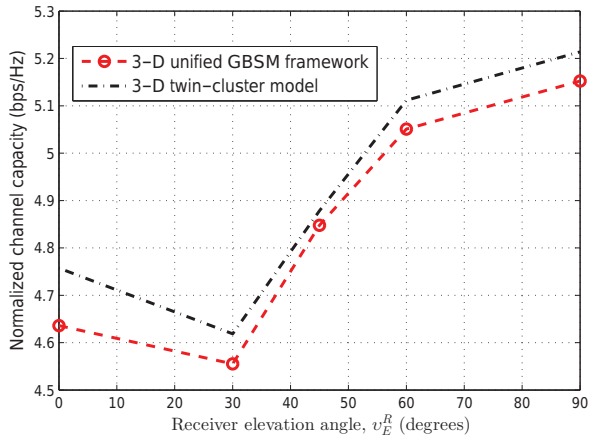


Fig. 3. Channel capacities of the 3-D twin-cluster channel model and the 3-D unified GBSM framework with different receiver elevation angles ($M_R = 8$, $M_T = 32$, $f_c = 2$GHz, $\|\mathbf{D}\| = 100$m, $\upsilon_A^R = \frac{\pi}{4}$, $\upsilon_A^T = \frac{\pi}{3}$, $\upsilon_E^T = \frac{\pi}{4}$, SNR $= 20$dB).

Channel capacities of the unified GBSM framework with normal and polarized antennas are shown in Fig. 4. The channel capacity with polarized antennas is lower than that with normal antennas. However, the dimensions of antenna arrays are halved because of the use of polarized antennas.

## IV. Conclusions

This paper has studied channel capacities of four stochastic massive MIMO channel models. It has been demonstrated that elevation angles can have significant impact on massive MIMO channel capacities. Therefore, it would be beneficial to consider 3-D models, rather than 2-D models, in massive MIMO channel modeling. For 3-D channel massive MIMO channel models, the size of an array can be halved with polarized antennas at the cost of slight channel capacity loss.

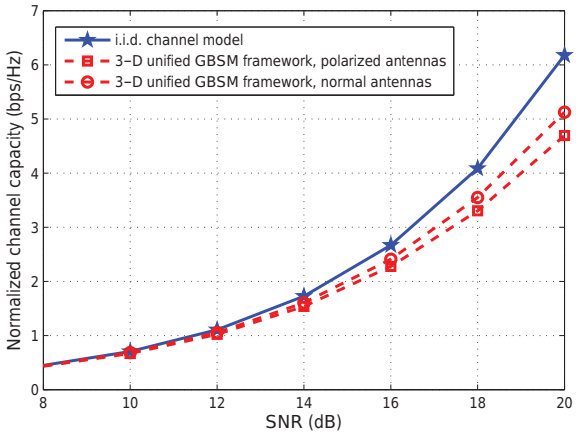


Fig. 4. Comparison of channel capacities of the unified GBSM framework for massive MIMO channel models with normal and polarized antennas ($M_R = 8$, $M_T = 32$, $f_c = 2$GHz, $\|\mathbf{D}\| = 100$m, $\upsilon_A^R = \frac{\pi}{4}$, $\upsilon_A^T = \frac{\pi}{3}$, $D_c^s = 100$m, $\varsigma = 7$s, $\upsilon_E^R = \frac{\pi}{4}$, $\upsilon_E^T = \frac{\pi}{4}$).


## Acknowledgment

The authors gratefully acknowledge the support of this work from the EPSRC TOUCAN project (No. EP/L020009/1), EU H2020 5G Wireless project (No. 641985), EU FP7 QUICK project (No. PIRSES-GA- 2013-612652), National Science and Technology Major Project (No. 2014ZX03003012-001), and 863 Project in 5G (No. 2014AA01A707).


## References


[1] S. Payami and F. Tufvesson, "Channel measurements and analysis for very large array systems at 2.6 GHz," in *Proc. EuCAP'16*, Prague, Czech Republic, Mar. 2012, pp. 433–437.

[2] X. Gao, F. Tufvesson, O. Edfors, and F. Rusek, "Measured propagation characteristics for very-large MIMO at 2.6 GHz," in *Proc. of the 46th Annual Asilomar Conference on Signals, Systems, and Computers*, California, USA, Nov. 2012, pp. 295–299.

[3] 3GPP T.S. 25.996, *Spatial channel model for multiple input multiple output (MIMO) simulations*, V11.0.0, 2012.

[4] WINNER D1.1.2 P. Kyosti, et al., "WINNER II channel models", ver 1.1, Sept. 2007. Available: https://www.ist-winner.org/WINNER2-Deliverables/D1.1.2v1.1.pdf

[5] Report ITU-R M.2135-1, "Guidelines for evaluation of radio interface technologies for IMT-Advanced", 2009.

[6] S. Wu, C. -X. Wang, H. Haas, el-H. M. Aggoune, M. M. Alwakeel, and B. Ai, "A non-stationary wideband channel model for Massive MIMO communication systems," *IEEE Trans. Wireless Commun.*, vol. 14, no. 3, pp. 1434–1446, Mar. 2015.

[7] S. Wu, C. -X. Wang, el-H. M. Aggoune, M. M. Alwakeel, and Y. He, "A non-stationary 3-D wideband twin-cluster model for 5G massive MIMO channels," *IEEE J. Sel. Areas Commun.*, vol. 32, no. 6, pp. 1207–1218, June 2014.

[8] A. A. M. Saleh and R. A. Valenzuela, "A statistical model for indoor multipath propagation," *IEEE J. Sel. Areas Commun.*, vol. 5, no. 2, pp. 128–137, Feb. 1987.

[9] S. Wu, C. -X. Wang, el-H. M. Aggoune, M. M. Alwakeel, and X. -H. You, "A unified framework for 5G wireless channel," *IEEE Trans. Wireless Commun.*, submitted for publication.

[10] S. Wu, C. -X. Wang, el-H. Aggoune, and M. M. Alwakeel, "A novel Kronecker-based stochastic model for massive MIMO channels," in *Proc. ICCC'15*, Shenzhen, China, Nov. 2015, pp. 1–6.

[11] C.-N. Chuah, D. N. C. Tse, J. M. Kahn, and R. A. Valenzuela, "Capacity scaling in MIMO wireless systems under correlated fading," *IEEE Trans. Inf. Theory*, vol. 48, no. 3, pp. 637–650, Mar. 2002.